Journal of Marine Systems 78 (2009) 59–76

Contents lists available at ScienceDirect

Journal of Marine Systems

journal homepage: www.elsevier.com/locate/jmarsys

High SST variability south of Martha's Vineyard: Observation and modeling study

Xiaodong Hong [a,*], Paul J. Martin [b], Shouping Wang [a], Clark Rowley [b]

[a] Naval Research Laboratory, Monterey, CA 93943, USA
[b] Naval Research Laboratory, Stennis Space Center, MS 39529-5004, USA

ARTICLE INFO

Article history:
Received 4 November 2008
Received in revised form 2 March 2009
Accepted 13 March 2009
Available online 27 March 2009

Keywords:
High SST variability
Tidal mixing
Atmospheric forcing
High model resolution

ABSTRACT

High, small-scale SST variability (6 °C over 5–10 km) observed South of Martha's Vineyard during the low-wind component of the Coupled Boundary Layers Air–Sea Transfer (CBLAST-Low) oceanographic field program in August 2003 is investigated using the Navy Coastal Ocean Model (NCOM), with atmospheric forcing provided by the Coupled Ocean/Atmosphere Mesoscale Prediction System (COAMPS®).[1] The ocean model includes tidal boundary forcing by the eight major tidal constituents, which is superimposed on the non-tidal lateral boundary conditions obtained from the 1/8° global NCOM real-time hindcast. The simulation is conducted with a high-resolution, 200-m grid, with bathymetry from the NGDC 3-arc-second Coastal Relief Model. The COAMPS fields, tidal forcing and NCOM results are evaluated with the CBLAST-Low observations and previous results. Both the simulation and observation analyses reveal that SST variability south of Martha's Vineyard is significant on August 18 and 25 and is strongly related to the cooling events on August 17 to 18 and August 24 to 25. The northeast winds passing through Muskeget Channel generate sharp horizontal SST gradients on August 18 by accelerating the westward transport of cold water from the cold, tidally-mixed Nantucket Shoals and by wind-induced upwelling and surface-cooling-induced vertical mixing. The mechanism of SST change on August 25 is differentiated from the change on August 18 by the northwest winds being unfavorable to the westward transport of cold water. The SST cooling on August 25 is mainly caused by local vertical mixing induced by heat lost.

Published by Elsevier B.V.

1. Introduction

Strong spatial and temporal variability of sea surface temperature (SST) over the waters south of Martha's Vineyard was observed during the CBLAST-Low field program during the summers of 2001, 2002, and 2003 (Edson et al., 2007). The horizontal distribution of SST in this area is highly non-homogeneous, with changes of up to 6 °C at the edges of the cold-water band (Fig. 1). These patterns of high SST variability do not, in general, linger more than a day. However, the high SST variability significantly modulated the air–sea heat exchange, with a dramatic change in the measured latent and sensible heat fluxes (nearly 150 W m^{-2} total) as the observation vessel moved across the narrow oceanic frontal zone (Edson et al., 2007). This substantial modulation has been studied by Vickers and Mahrt (2006) through analysis of aircraft data. They found that the momentum and sensible and latent heat fluxes change greatly when the SST changes exceed 1 °C in amplitude over a distance of about 8 km.

The processes producing this strong SST gradient may involve the tide since the tide is a primary forcing for the regional circulation through tidally-induced vertical mixing and topographic-related tidal residual currents (He and Wilkin, 2006). Tidal mixing is sufficiently strong on the relatively shallow Nantucket Shoals that the water column is well mixed in the vertical throughout the summer, thereby maintaining a perpetually cool SST over Nantucket Shoals and an oceanic front on the west side of Nantucket Shoals despite significant, sustained, surface heating (Wilkin, 2006). One branch of the tidal residual mean current flows westward, advecting the tidally-mixed cold water from Nantucket Shoals to the midshelf south of Martha's Vineyard (He and Wilkin, 2006). However, the cold waters carried by the tidal mean flow are warmed under the influence of surface heating during the summer.

The predominant winds in the study area during the summer are from the SW, with wind speeds typically reaching 2–6 m/s according to the accumulated data from the Martha's Vineyard Coastal Observatory (MVCO) (Edson et al., 2007). The surface waters warm steadily throughout the summer in response to net air–sea heating, with net advection generally playing a modest role in cooling the water column south of Martha's Vineyard and west of Nantucket Shoals (Wilkin, 2006). Strong thermal stratification is a dominant feature in this region.

The high SST variability in Fig. 1 shows that a narrow tongue of cold water breaks the thermal stratification south of Martha's Vineyard and connects with the tidally-mixed water along the flank of Nantucket Shoals. These large, horizontal SST gradients are observed only on

* Corresponding author. 7 Grace Hopper Avenue, Monterey, CA 93955, USA. Tel.: +1 831 656 4746; fax: +1 831 656 4769.
E-mail address: xd.hong@nrlmry.navy.mil (X. Hong).

[1] COAMPS® is a registered trademark of the Naval Research Laboratory.

0924-7963/$ – see front matter. Published by Elsevier B.V.
doi:10.1016/j.jmarsys.2009.03.001

Report Documentation Page

Form Approved
OMB No. 0704-0188

1. REPORT DATE	2. REPORT TYPE	3. DATES COVERED
02 MAR 2009		**00-00-2009 to 00-00-2009**

4. TITLE AND SUBTITLE	5a. CONTRACT NUMBER
High SST variability south of Martha's Vineyard: Observation and modeling study	5b. GRANT NUMBER
	5c. PROGRAM ELEMENT NUMBER
6. AUTHOR(S)	5d. PROJECT NUMBER
	5e. TASK NUMBER
	5f. WORK UNIT NUMBER
7. PERFORMING ORGANIZATION NAME(S) AND ADDRESS(ES) **Naval Research Laboratory,7 Grace Hopper Avenue,Monterey,CA,93955**	8. PERFORMING ORGANIZATION REPORT NUMBER
9. SPONSORING/MONITORING AGENCY NAME(S) AND ADDRESS(ES)	10. SPONSOR/MONITOR'S ACRONYM(S)
	11. SPONSOR/MONITOR'S REPORT NUMBER(S)

12. DISTRIBUTION/AVAILABILITY STATEMENT
Approved for public release; distribution unlimited

13. SUPPLEMENTARY NOTES

14. ABSTRACT
see report

15. SUBJECT TERMS

16. SECURITY CLASSIFICATION OF:			17. LIMITATION OF ABSTRACT	18. NUMBER OF PAGES	19a. NAME OF RESPONSIBLE PERSON
a. REPORT **unclassified**	b. ABSTRACT **unclassified**	c. THIS PAGE **unclassified**	**Same as Report (SAR)**	**18**	

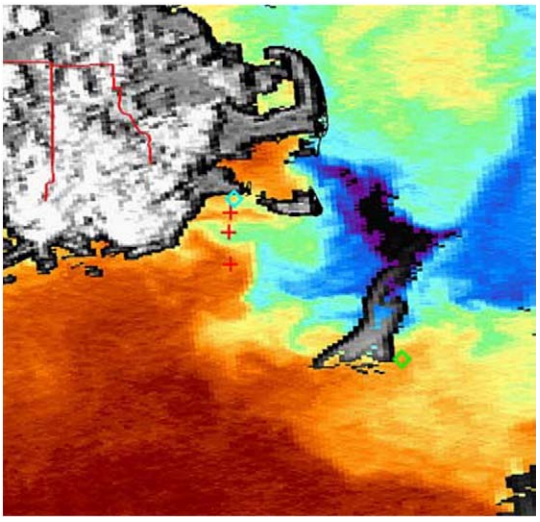

Fig. 1. AVHRR image of the CBLAST experimental area collected at 21:43 UT on August 18, 2003 (courtesy of Thompson et al., 2007).

some days, therefore, the processes involved may not only relate to the horizontal advection of the tidal mean flow but also other possible processes associated with surface forcing, such as local vertical mixing and upwelling by the winds or local surface cooling via air–sea surface heat fluxes.

In this study, we examine the mechanism of the formation of high SST variability south of Martha's Vineyard during August 2003 using the Navy Coastal Ocean Model (NCOM) with high horizontal resolution and observations taken during the CBLAST-Low period. The purpose is to examine the main dynamics and physical processes driving the formation of this small-scale feature and to understand the relative importance of the individual processes involved.

Brief descriptions of NCOM, the atmospheric forcing, and the model configuration are given in Section 2. Tidal analysis of the barotropic tidal residual current and the tidal amplitude and phase are presented in Section 3. The observed high SST variability is reviewed in Section 4. In Section 5, the atmospheric forcing is evaluated with a focus on the periods of high SST variability. In Section 6, the NCOM results are compared with the CBLAST observations. In Section 7, the mechanism of the high SST variability is investigated through the model results. Section 8 contains the summary.

2. Model configuration

2.1. The ocean model NCOM

NCOM is a three-dimensional, primitive-equation, free-surface model using the hydrostatic, Boussinesq, and incompressible approximations (Martin 2000; Morey et al., 2003). NCOM is designed to offer the user a range of numerical choices in terms of parameterizations, numerical differencing, and vertical grid structure. It uses a hybrid vertical coordinate system, which allows for the use of all sigma-levels, all z-levels, or a combination of sigma-levels for the upper ocean and z-levels below a specified depth. The model equations are solved on a staggered Arakawa C-grid. Temporal differencing is leap-frog with an Asselin filter to suppress time splitting. Spatial averages and finite differences are mainly second order, with options for higher-order formulations for some terms. The propagation of surface waves and vertical diffusion are treated implicitly. For this study, the Mellor-Yamada Level 2.5 turbulence scheme is used for vertical mixing and a third-order upwind scheme is used for advection. NCOM forcing can include surface atmospheric fluxes, lateral open boundary conditions, tides, and river and runoff discharges.

NCOM has been applied to a number of regions, including the Adriatic Sea (Pullen et al., 2003; Martin et al., 2006) and Monterey Bay (Hong et al., 2009; Shulman et al., 2007) to study the evolution of fine-scale oceanic features under atmospheric forcing, and the Gulf of Lion to study the effects of time variation of the surface buoyancy flux on the formation of deep-water convection during the winter season (Hong et al., 2007). In a coastal application of ocean data assimilation, NCOM is used in the Navy Coupled Ocean Data Assimilation (NCODA) system (NCODA, Cummings, 2005) as a forward model for a sequential update cycle (Hong et al., 2009). A recent application is the development of NCOM ensemble forecasting (Hong and Bishop, 2005) using the ensemble transform technique (Bishop and Toth, 1999) and adaptive sampling for coastal observations (Hong and Bishop, 2006) using the ensemble transform Kalman filter method (Bishop et al., 2001).

2.2. Atmospheric forcing

The surface atmospheric forcing is from a real-time forecast using the Navy's Coupled Ocean/Atmosphere Mesoscale Prediction System (COAMPS) (Hodur et al., 2002) for the CBLAST-Low field program from July to August 2003. COAMPS was run twice daily using 3 nested grids with horizontal grid increments of 3, 9, and 27 km, respectively. The surface forecast fields from the innermost grid were output at hourly intervals and used to force NCOM.

The atmospheric forcing for NCOM consists of the surface air pressure, wind stress, air–sea heat flux, and effective surface salt flux for the momentum, temperature, and salinity equations. The surface latent and sensible heat fluxes can use the COAMPS-computed values (used in this study) or be computed interactively from the COAMPS wind speed, air temperature, and relative humidity and the NCOM-predicted SST using standard bulk formulas and the drag coefficient of Kondo (1975) (Martin and Hodur, 2003). The surface salt flux for NCOM is calculated from the latent heat flux and the COAMPS precipitation. The extinction of solar radiation in seawater as classified by Jerlov (1976) is used to define the subsurface penetration of the COAMPS solar radiation.

2.3. Model configuration

The ocean model was run on a domain matching the size of the COAMPS innermost grid (grid 3) with 1351×1351 grid points in the horizontal at a resolution of 200 m (Fig. 2). The vertical grid is logarithmically stretched from the surface downward with an upper-layer thickness of 1 m and a maximum depth of 1365 m. There are a total of 32 layers with a switchover from sigma to z-level vertical coordinates at about 115-m depth. The vertical grid in most of the model domain is sigma coordinate since the depths are mostly less than 100 m. The model bathymetry (Fig. 1) was obtained by a cubic spline interpolation of data from the 3-arc-second Coastal Relief Model developed by NOAA's National Geophysical Data Center (NGDC) (Divins and Metzger, 2008). The bathymetry is fairly complex, with many sand ridges in the area of Nantucket Shoals. The water depths are generally less than 40 m on the shoals. To the east of Nantucket Shoals is a 60-m deep channel called the Great South Channel, to the northeast is the Gulf of Maine (GOM) with depths greater than 200 m, and to the west is the Middle Atlantic Bight (MAB) with relatively smooth bathymetry. The model domain includes a portion of the shelf break near the south boundary so that interaction between the cool continental shelf water and the more saline continental slope water can occur.

The ocean model uses the 1/8° global NCOM real-time hindcast fields with sea surface elevation, temperature, salinity, and currents for initial and lateral boundary conditions (Barron et al., 2006). Tidal forcing includes both elevation and transports for four diurnal (K_1, O_1, P_1, and Q_1) and four semidiurnal (K_2, M_2, N_2, and S_2) constituents from

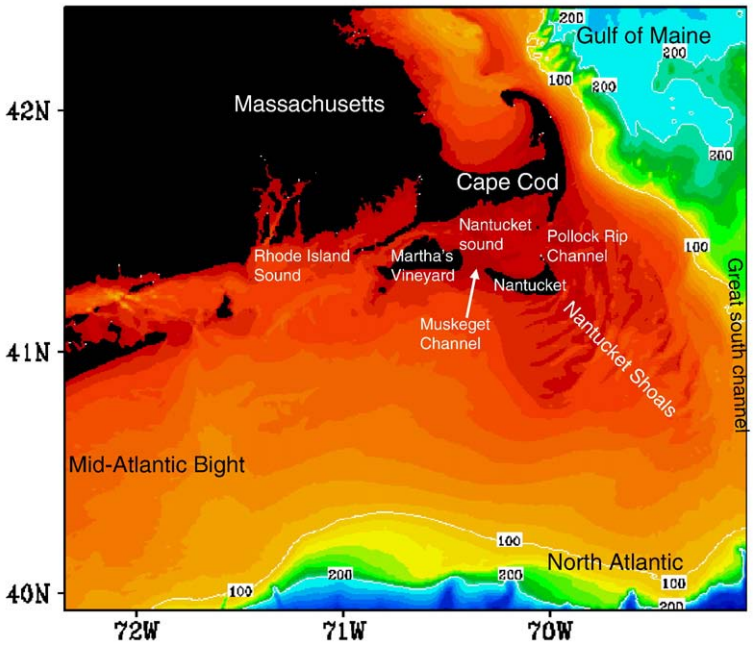

Fig. 2. Model domain and bathymetry. The white contour lines denote 100- and 200-m isobaths.

the North Atlantic tidal database developed at Oregon State University (Egbert et al., 1994). The tidal elevation and transports are superimposed on the non-tidal lateral boundary conditions from global NCOM. Tidal potential forcing is used in the interior, though its effect in this shallow, limited-area domain is small.

3. Tidal analysis

Since tidal forcing is very important for the regional circulation on the southeast New England shelf (He and Wilkin, 2006), the model includes a good representation of the tides. In this section, the model

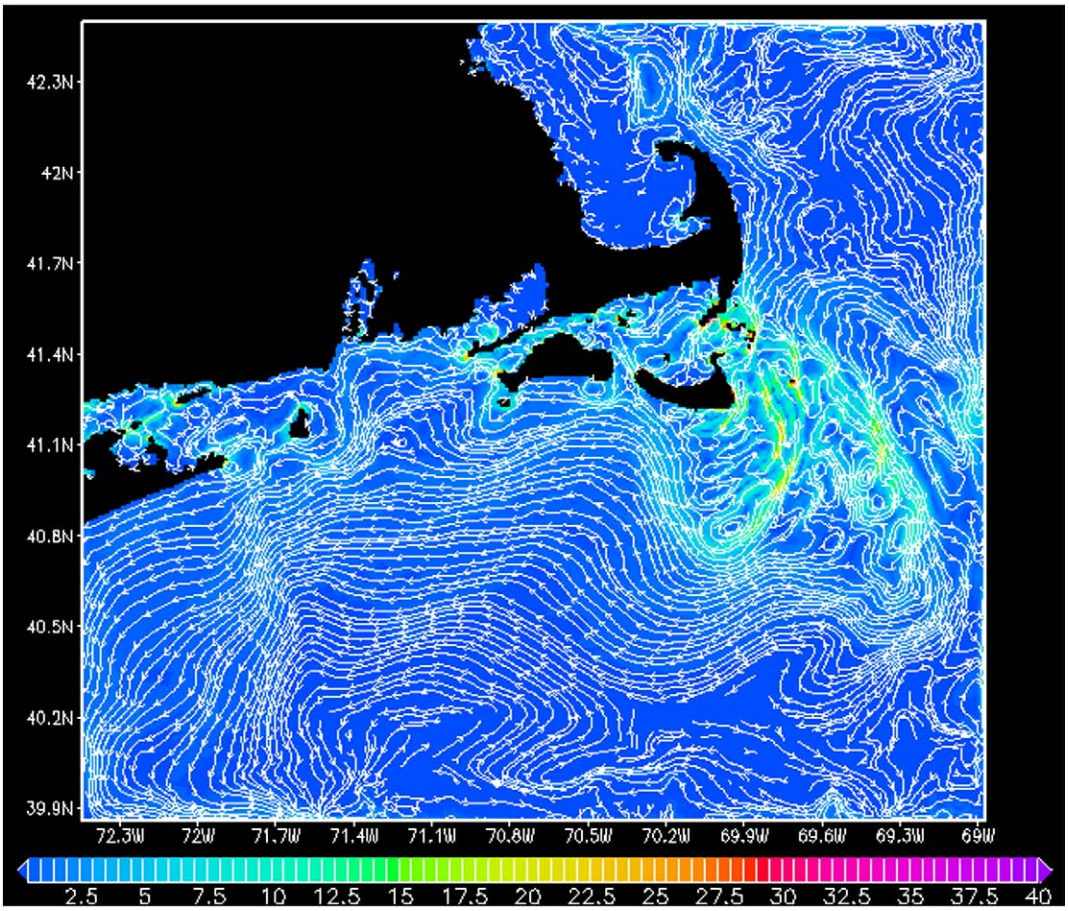

Fig. 3. Barotropic tidal residual current obtained from time-averaging a one-layer tidal simulation with eight tidal constituents over a period of about 100 days.

tides are analyzed and compared with the results from the data-assimilative modeling study of He and Wilkin (2006). In their study, in situ observations, including the tidal harmonics of the 5 major tidal constituents [M_2, S_2, N_2, O_1, and K_1] were analyzed from 15 sets of coastal sea-level and bottom pressure gauges and assimilated via an inversion for the barotropic tidal open boundary conditions.

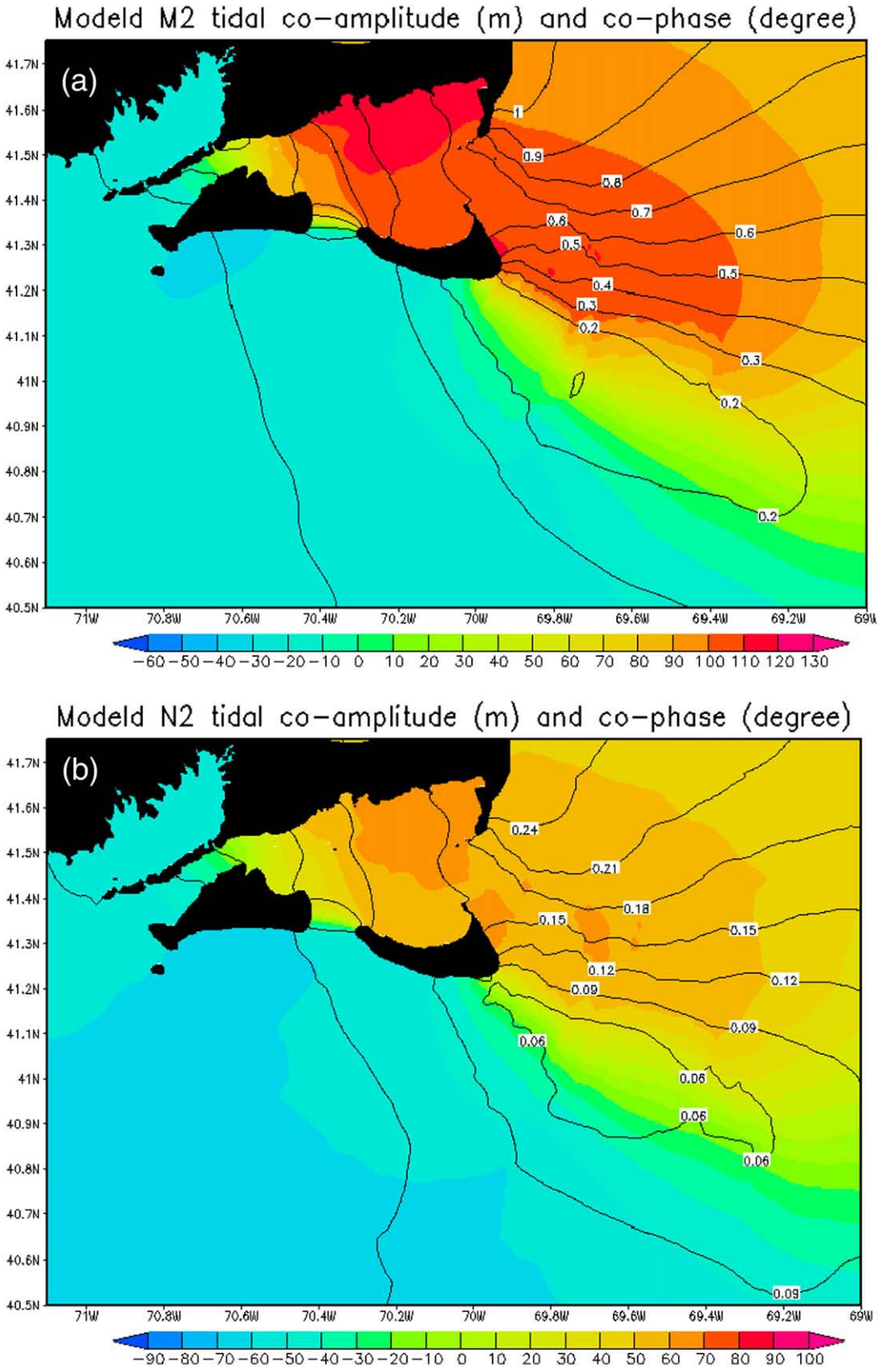

Fig. 4. Modeled tidal amplitude (contour) and phase (color) for (a) M_2 and (b) N_2 constituents. (For interpretation of the references to color in this figure legend, the reader is referred to the web version of this article.)

The barotropic tidal residual currents for the model domain were computed by time-averaging a one-layer tidal simulation with the eight tidal constituents that were used over a period of about 100 days. The model density field for this simulation was set to be homogenous so that no density currents would be induced. The residual currents were time-averaged from the hourly velocities output over the last 95 days of the simulation, i.e., over about 200 M_2 cycles. With the highly-resolved bathymetry at 200-m resolution, the nonlinear interaction of the tidal flow and the complex bottom generates strong tidal residual currents, with a maximum speed reaching 20 cm s^{-1} (about 17 km day^{-1}) to the east of Nantucket Island (Fig. 3). The general features of the tidal residual current are similar to those from He and Wilkin (2006), including the flow entering the New England Shelf from the east and from the Great South Channel. The results here, however, show more detailed and complex structures. The scales of these structures are small, with many cyclonic eddies located at positions related to the locations of the sand ridges. The overall spatial pattern of the tidal residual current strongly resembles the pattern of the bottom topography.

Equilibrium tidal amplitudes and phases for all 8 tidal constituents were analyzed from the model output using least squares fitting. The amplitude and phases for the M_2 and N_2 tidal constituents are displayed in Fig. 4. These tidal amplitudes and phases are very similar to the results obtained by He and Wilkin (2006). The amplitude for the M_2 tide decreases from 0.4 m offshore of Martha's Vineyard to about 0.1 m over Nantucket Shoals, then rapidly increases to about 1 m toward the Gulf of Maine (Fig. 4a). The M_2 tidal phase is also comparable in which its value increases slightly from −10° to 0° south of Nantucket, then changes dramatically to over 100° in the north. The amplitude of the N_2 tide has smaller amplitude (Fig. 4b), being only about 10–20% of M_2. However, the spatial patterns for the amplitude and phase of N_2 are similar to those for M_2. These semidiurnal tides have a common feature, a local amplitude minimum over Nantucket Shoals due to the 90–120° elevation phase lag and counteracting tides between the MAB and the GOM as pointed out by He and Wilkin (2006).

4. Observed high SST variability

The SST variability mapped in Fig. 5 is an infrared radiometric (IR) measurement by a Pelican aircraft, a modified Cessna 337 with only a pusher engine. This is a highly instrumented research aircraft operated by the Center for Interdisciplinary Remotely-Piloted Aircraft Studies (CIRPAS) at the Naval Postgraduate School in Monterey, California. The majority of the Pelican IR SST measurements are located to the south of Martha's Vineyard.

The Pelican took off at 1415 and landed at 1819 UTC (local Eastern Daylight Saving Time equals UTC minus 4 h) on August 15, 2003 and the measured SST is mapped in Fig. 5a (CBLAST low log, 2003). Winds were low-to-moderate throughout the day, with wind speeds of 2.5–4.5 m s^{-1} in the early morning hours, decreasing to speeds of 1–2 m s^{-1} by about noon local time. The winds were from the south/southwest, the prevailing wind directions. The low winds and strong daytime heating led to the development of strong, shallow temperature stratification, with a temperature gradient of about 2 °C over the upper 2 m (Farrar et al., 2007). This is a typical summer SST pattern, in which net air–sea heat fluxes produce strong thermal stratification south of Martha's Vineyard.

The SST measured on August 18, 2003 shows a cold anomaly (Fig. 5b), a tongue of cold water extending across the central part of the mapped area. The cold tongue has an average width of 8 km in the north–south direction, with a maximum temperature change of 6 °C over 5 km at its southern end where it meets the warm waters to the south. The Pelican took off at 1324 and landed at 1738 UTC. The local winds at this time were from the northeast, i.e., opposite the prevailing wind direction in summer.

The SST on August 23 and 25 displayed in Fig. 5c and d depicts another incident in which the strong, stratified, warm waters south of Martha's Vineyard are transformed into colder water similar to that seen on August 15 and 18 in Fig. 5a and b. The narrow, cold-water band southeast of Nantucket Island may be a portion of the cold-water intrusion from the tidally-mixed cold-water pool on the flank of Nantucket Shoals to the south of Martha's Vineyard. The curving band of cold water denotes the path of the cold-water transport.

Time series and flux data from repeated low-level-flight measurements across the front on August 18, 2003 show that turbulence is abruptly suppressed (enhanced) as the aircraft moved from the warm (cold) to the cold (warm) waters. This leads to a reversal in the stability of the atmospheric boundary layer in a very short distance (Khelif et al., 2004; Edson et al., 2007).

5. Variability of atmospheric forcing

From the observations, the response of the atmospheric boundary layer to the abrupt SST variation is evident (Edson et al., 2007). But how does the strong spatial variability of the wind stress and air–sea heat fluxes modulate the upper-ocean processes? How is the narrow, cold-water band south of Martha's Vineyard formed? Does any linkage exist between the surface forcing and the high SST variability? To answer these questions, we first examine the atmospheric conditions at the times that the narrow, cold-water transport occurs through both the observations and the COAMPS forecast.

The COAMPS-predicted sensible and latent heat fluxes and wind speed in the east–west and north–south directions are compared with observed values taken at the CBLAST Air–Sea Interaction Tower (ASIT, marked by a black star in Fig. 1). All the predicted and observed time series are filtered using a second-order Butterworth low-pass filter with a 21-hour cutoff (Fig. 6). The positive heat fluxes mean the ocean is gaining heat and vice versa. The directions for both the predicted and observed winds are plotted as wind barbs at the bottom of the figure.

The observations show that the predominant winds in the study area are from the southwest/west, with wind speeds typically reaching 2–6 m s^{-1} (Edson et al., 2007) and the local heat balance leads to air–sea warming throughout the summer (Wilkin, 2006). These conditions can be found in Fig. 6 for most of the times during August 2003, except for two time periods from August 17 to 18 and from August 24 to 25 when the winds blow from the northeast and northwest, respectively. These two time periods with winds that are variant from the predominant winds are shaded in the figure for the air–sea heat fluxes and wind components so that the corresponding changes of the winds and air–sea heat fluxes can be compared. The ocean loses heat during these periods, indicating cooling events associated with the passage of storms and atmospheric fronts. The air–sea cooling is more significant from August 24 to 25 than from August 17 to 18, with a maximum difference of about 200 W m^{-2} between them based on the ASIT observations.

The daily mean surface values in Fig. 7 show that on August 16 and 20 the ocean received heat fluxes of 90 to 280 W m^{-2}, with the greatest amount in the tidal-mixing-induced perpetually cool SST area over the Nantucket Shoals (He and Wilkin, 2006; Wilkin, 2006; Edson et al., 2007). The distribution of atmospheric sea-level pressure is a typical summer pattern with low in the north and high in the south, accompanied by west/southwest winds. However, when a cooling event associated with a high-pressure system passage occurs, winds blow from the northeast on August 18 (Fig. 7b). The air–sea heat flux is significantly reduced and becomes negative (the ocean loses heat) due to the cooler air that has moved into the area. The winds are intensified by a gap-type wind effect when passing through the Muskeget Channel, causing larger heat loss than in other areas. The heat loss is up to 120 W m^{-2} in the southwest area, replacing the heat

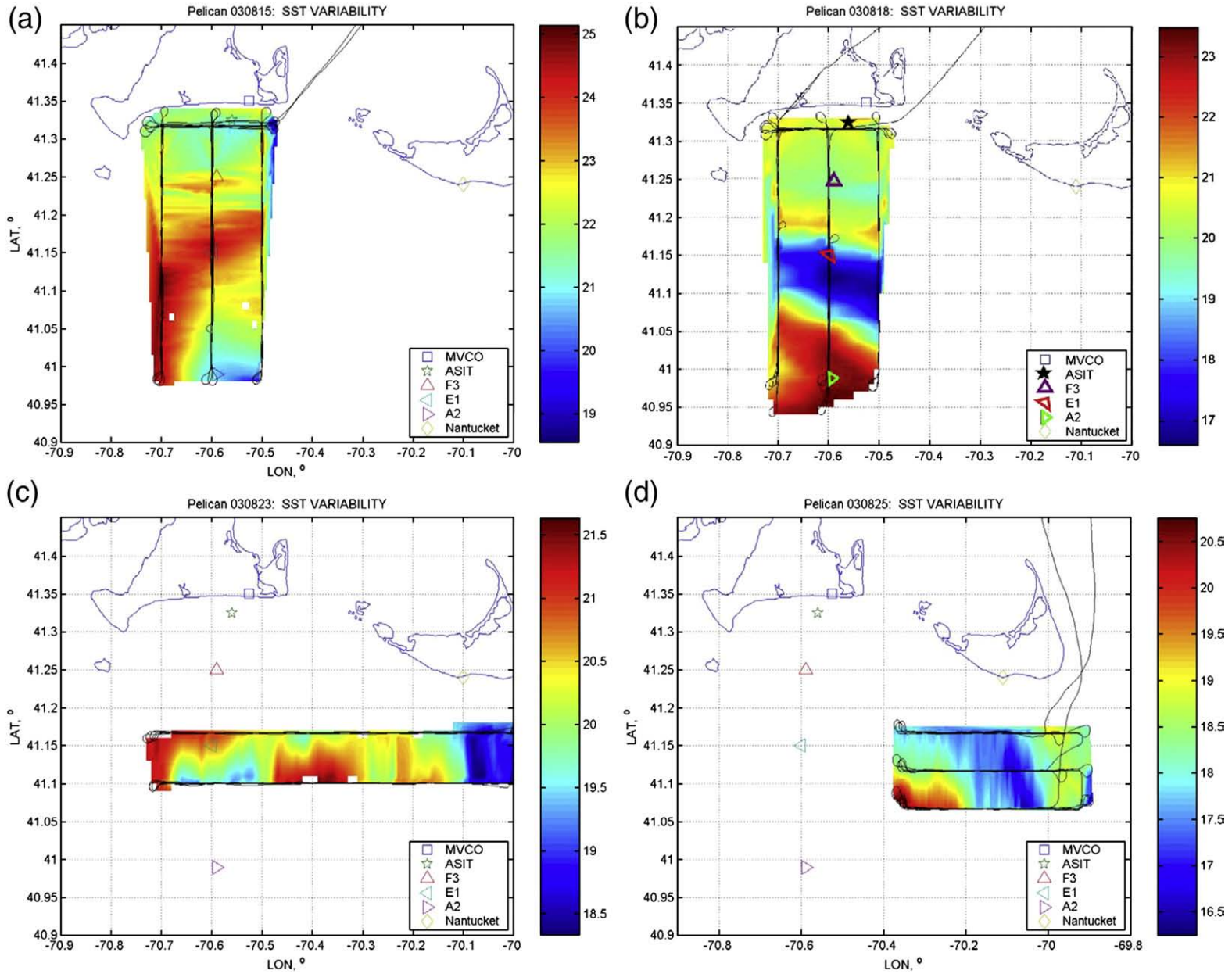

Fig. 5. SST variability as measured by the CIRPAS Pelican aircraft IR pyrometer in CBLAST-Low on (a) August 15, (b) August 18, (c) August 23 and (d) August 25, 2003. The star south of Martha's Vineyard marks the location of the ASIT, the purple, red and green triangles show the IMET moorings for the locations of F, E and A, respectively (all images are from http://wave.eng.uci.edu/files/cblast/flights/). (For interpretation of the references to color in this figure legend, the reader is referred to the web version of this article.)

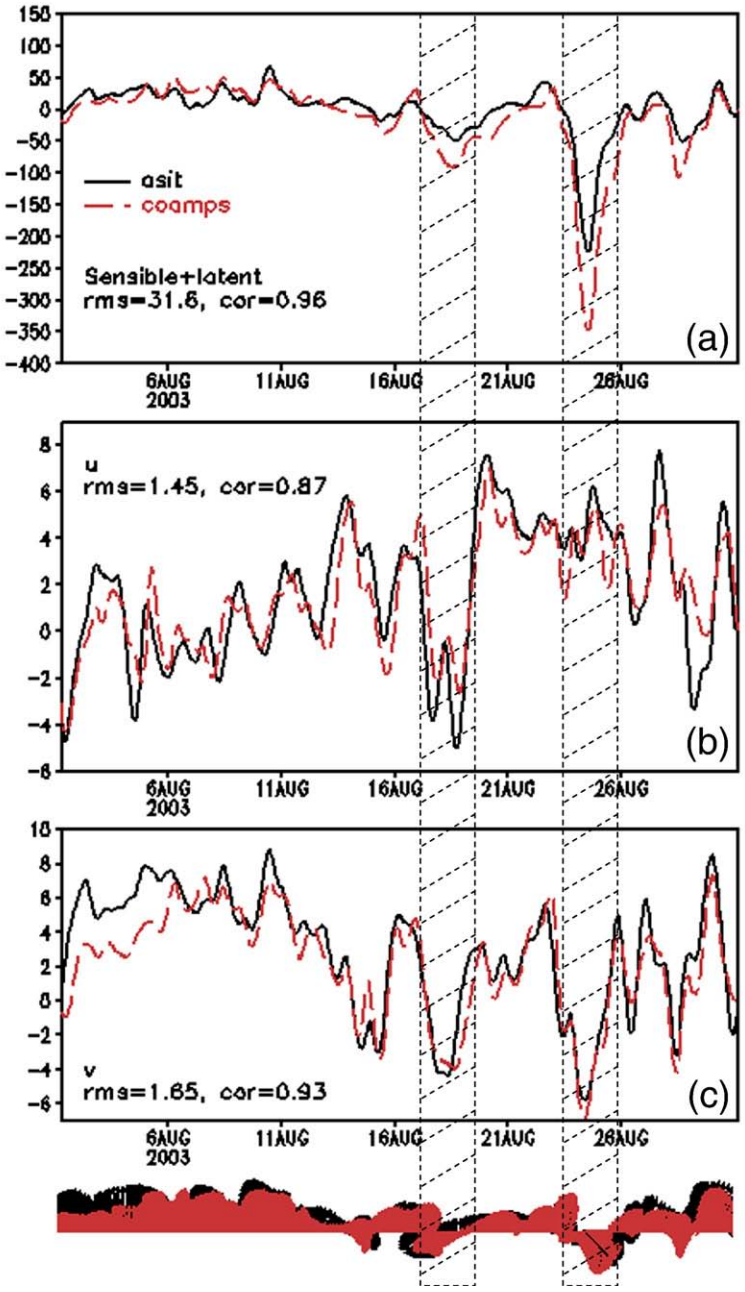

Fig. 6. Time series of ASIT-observed (black solid lines) and COAMPS-predicted (red dashed-lines) (a) sensible and latent heat fluxes, (b) wind speed in the east–west direction, and (c) wind speed in the north–south direction. Vectors showing the observed and predicted wind directions are shown at the bottom of the figure. The shaded areas show the times when the winds blow from the north or northeast directions. The position of the ASIT is marked by a black star in Fig. 1. (For interpretation of the references to color in this figure legend, the reader is referred to the web version of this article.)

gain of up to 160 W m^{-2} on August 16. The area of heat loss spreads out in a southeast direction following the direction of the winds.

West/southwest winds continue for a few days after the cooling event on August 18. The area gains heat with a maximum heating of over 300 W m^{-2} in the cold-pool region on August 23 (Fig. 8a). On August 24 another cooling event occurs, inducing a larger heat loss for the ocean (Fig. 8b). The daily mean wind stress on August 24 is about 0.1 N m^{-2} larger than that on August 18. The winds associated with the low-pressure system passage on August 24 are from the northwest, whereas, the winds associated with the high-pressure system on August 18 are from the northeast. The maximum heat loss over the southwest area on August 24 is 350 W m^{-2}, about 230 W m^{-2} more than that on August 18. The heat gain in the cold-pool area reduces to 120 W m^{-2}, about 180 W m^{-2} less than that on August 23. The modulation of the air–sea heat fluxes by the two islands can be clearly seen in Fig. 8b. After the passage of the cool front, the air–sea heat fluxes resume the normal air–sea warming conditions of the summer season, with low sea-level pressure in the north and high pressure in the south (Fig. 8c).

The COAMPS real-time forecast during CBLAST-Low was evaluated using both mean and turbulence measurements collected during the 2002–2003 experiments (Wang et al., 2004). Here we compare the COAMPS forecast with the observations at the ASIT site (Fig. 6 and Table 1). The statistical results show that the mean and standard deviation of the sensible and latent heat fluxes produced by COAMPS have larger values than the ASIT observations, with a Root-Mean-Square (RMS) error of about 31 W m^{-2}. The correlation coefficient for the COAMPS sensible and latent heat fluxes relative to the

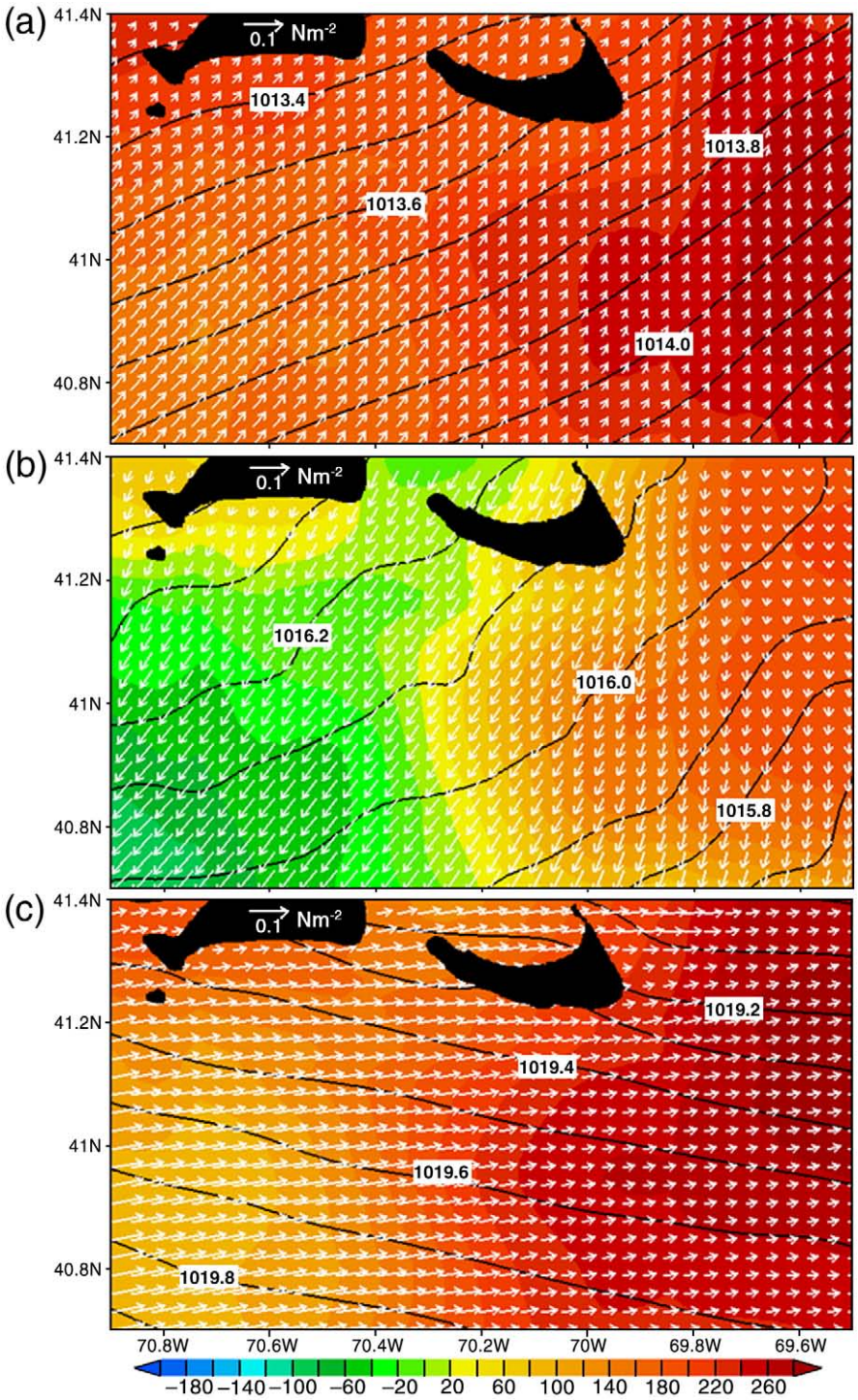

Fig. 7. Daily mean surface heat flux (W m^{-2}, color contours), sea-level pressure (mb, black contour lines) and wind stress (N m^{-2}, white vectors) from the COAMPS forecast are plotted for (a) August 16, (b) August 18, and (c) August 20. (For interpretation of the references to color in this figure legend, the reader is referred to the web version of this article.)

observations at the ASIT site is 0.96. Thus, the COAMPS-predicted air–sea heat fluxes are comparable with the observations at the ASIT site.

The COAMPS-predicted wind-speed mean values and standard deviations for the *u* and *v* components at the ASIT site are similar to the observations. Both the mean and standard deviation from COAMPS are slightly smaller than for the ASIT observations. The correlation coefficients for both components relative to the observations are 0.87 and 0.93, respectively. The RMS errors for both components are 1.45 and 1.65 m s^{-1}, respectively, which are within the ranges of other evaluations of COAMPS with observations (Chao et al., 2003; Pullen et al., 2003; Nachamkin, 2004). These agreements are consistent with the results from evaluation of the COAMPS real-time forecast for the CBLAST-Low summer experiments in 2002/2003 (Wang et al., 2004).

The winds deviated from their predominant directions and the air–sea heat fluxes deviated from their warming trend over the synoptic (2–10 day) weather band as a result of the passage of atmospheric

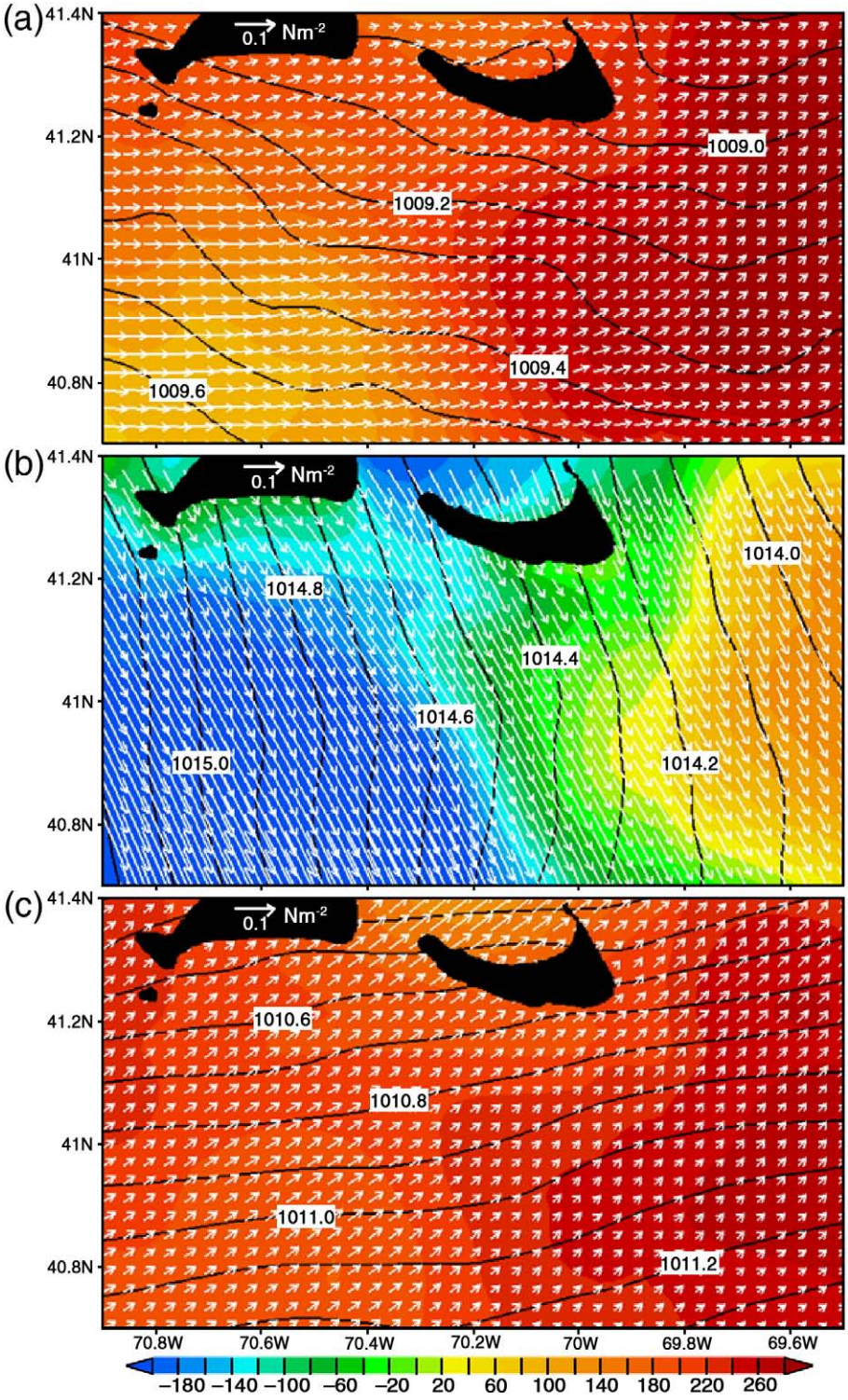

Fig. 8. Same as Fig. 10 except for (a) August 23, (b) August 24, and (c) August 27.

fronts from August 17 to 18 and from August 24 to 25, which is coincident with the ocean cooling events on August 18 and 25 south of Martha's Vineyard. These variant atmospheric conditions are important in modulating the local ocean conditions and may have a connection with the high SST variability associated with the narrow cold-water transport. The NCOM numerical simulation covering the month of August 2003 and including these two cooling events will aid in revealing this connection.

6. Comparison of NCOM results with observations

The NCOM model configured as described in Section 2 was run for two months from July 1 to August 31, 2003. The mean fields from the model simulation during August have major features similar to the simulation made by Wilkin (2006) using the Regional Ocean Modeling System (ROMS). These include a perpetually cold SST induced by tidal mixing on the east flank of Nantucket Shoals, a strong,

tidally-rectified, anticyclonic flow encircling the Nantucket Shoals, and strong stratification south of Martha's Vineyard.

The high SST variability observed by the CIRPAS Pelican IR pyrometer on August 18 (Fig. 5b) and August 25 (Fig. 5d) was compared with the NCOM-predicted SST variability. The snapshots of SST for both days are plotted and the partial aircraft tracks corresponding to the tracks in Fig. 5b and d are marked as straight lines with arrows denoting the track direction. The results from the simulation are able to show the sharp surface temperature changes south of Martha's Vineyard. The cold-water tongue observed on August 18 (Fig. 5b) is caused by an intrusion of cold water into the summer-stratified warm water from the cold pool on the east flank of Nantucket Shoals (Fig. 9a). The cool-water transport follows a narrow path and bends due to the structure of the bottom topography. However, the cold tongue center, which is located at about 41.2°N, is slightly north of that observed at about 41.1°N (Fig. 5b).

The observed SST variability southeast of Nantucket Island on August 25 (Fig. 5d) is also related to the cold-water transport (Fig. 9b). The SST in the area marked by the tracks in Fig. 9b shows similarity to that observed in Fig. 5d, with a sharp SST gradient on the west side of Nantucket Shoals. The transport path is less organized and the resulting horizontal SST gradient south of Martha's Vineyard is smaller than that on August 18. The reasons will be further investigated in the following sections.

The NCOM-simulated and Pelican-observed SST were compared for selected segments of the flight tracks shown in Fig. 9. The NCOM SST agrees better with the observed SST for August 18 (Fig. 10a) than for August 25 (Fig. 10b). The mean difference between the model-simulated and aircraft-observed SST for the selected tracks shown in Fig. 9 is only 0.01 °C for August 18 but is 0.83 °C for August 25 (Table 2). The standard deviation of the SST along the selected tracks on August 18 is larger than that on August 25, indicating larger horizontal gradients of SST on August 18. The simulation is able to capture this variability as shown in Fig. 9. The RMS error on August 18 is smaller than that on August 25. In concordance with the error, the correlation coefficient of the simulated SST relative to the observed SST reaches 0.86 on August 18, about 20% larger than that on August 25.

We further validated the NCOM-simulated SST for the month of August 2003 using the observations at the ASIT and at the air–sea interaction meteorological (IMET) moorings A, E, and F in Fig. 11. The locations of the ASIT and the IMET moorings are marked in Fig. 5b. Mooring E is located in the northern part of the cold-water band and mooring F is located just north of the cold-water band. However, the slightly northward positioned cold-water band from the NCOM simulation results in mooring F being located in the path of and mooring E being located south of the model-simulated cold-water band. The displacement of the model-simulated cold-water band will tend to increase the differences between the model simulation and the observations at the moorings.

The results from the NCOM forecast and from the ASIT and IMET moorings are comparable, with the correlation coefficients equal to or exceeding 0.8 and the RMS errors smaller than the standard deviations (Table 3). Relatively small RMS errors of 0.56 °C are obtained at the ASIT and at mooring F. The observed and predicted SST variability at the ASIT site during the month of August 2003 are similar, with standard deviations of 0.8 and 0.9 °C, respectively. The agreement between the observed and predicted SST at mooring F is good most of the time, except during the cool air intrusion from August 17 to 18. The model predicts about a 1.5 °C cooler SST than observed due to the northward displacement of the model-simulated path of the cold-water transport. Similar errors caused by this displacement occur at the A and E moorings. Both of these locations have predicted SST warmer than observed during the intrusion of the cold air.

The above comparisons among the aircraft IR, the mooring, and the model SST have not taken into account the discrepancy between the skin and bulk temperatures. The temperature measured by an infrared radiometer represents the radiometric temperature within the conductive diffusion-dominated sublayer at a depth of approximately 10–20 μm. This is referred to as the skin temperature and usually is cooler than the subskin temperature beneath (Donlon et al., 2007). An in situ measurement within the upper few meters of the water column is typically reported as the "bulk" SST. At night and when wind mixing is strong, the bulk SST is the same as the temperature at the base of the subskin layer. However, when daytime solar shortwave radiation penetrates to heat the water below the skin layer, and if wind mixing is weak, stable stratification develops in the upper few meters of the water column, in which the temperature increases towards the sea surface and a diurnal thermocline is formed. NCOM is capable of simulating a shallow surface layer as thin as the thickness of its uppermost layer, which in this study is 1 m thick. Therefore, the NCOM SST is a bulk SST that is more comparable with the in situ measurement.

7. Ocean response to the two cooling events

In this section we will focus on the relationship between the horizontal and vertical structures of the local ocean circulation and the two cooling events from August 17 to 18 and from August 24 to 25.

7.1. Cooling event from August 17 to 18, 2003

The wind direction in the study area changed from southwest before (August 16) to northeast during (August 18) to west after (August 20) the August 17–18 cooling event (Fig. 7). The winds from the southwest before the cooling event are unfavorable for the westward advection of cold water that originated from the cold pool on the flank of Nantucket Shoals. The advection progresses slowly since the currents induced by the zonal components of these winds have direction opposite that of the cold-water transports (Fig. 12a). Warm water exits Nantucket Sound through Muskeget Channel, indicated also by Wilkin (2006) from their observation and modeling study. According to Wilkin (2006), the warm water encroached on the islands is the result of eddy heat transport on each ebb tide. The eddy flux of heat sustains the adverse temperature gradient opposed by the local mean flow and forms a region of warm water trapped against the south coast of Martha's Vineyard. Strong stratification exists south of Martha's Vineyard, but relatively weaker stratification occurs in the path of the cold-water transport between the 25- and 40-m isobaths where the thermoclines tilt upwards (Fig. 12b). The

Table 1
Comparison of ASIT-observed and COAMPS modeled heat fluxes and wind-speed components.

	Sensible and latent ($W\ m^{-2}$)		u-component ($m\ s^{-1}$)		v-component ($m\ s^{-1}$)	
	ASIT	COAMPS	ASIT	COAMPS	ASIT	COAMPS
Mean	−0.87	−16.06	1.78	1.62	2.99	2.16
Standard deviation	40.12	64.04	2.86	2.31	3.42	3.10
Correlation	0.96		0.87		0.93	
RMS error	31.69		1.45		1.65	

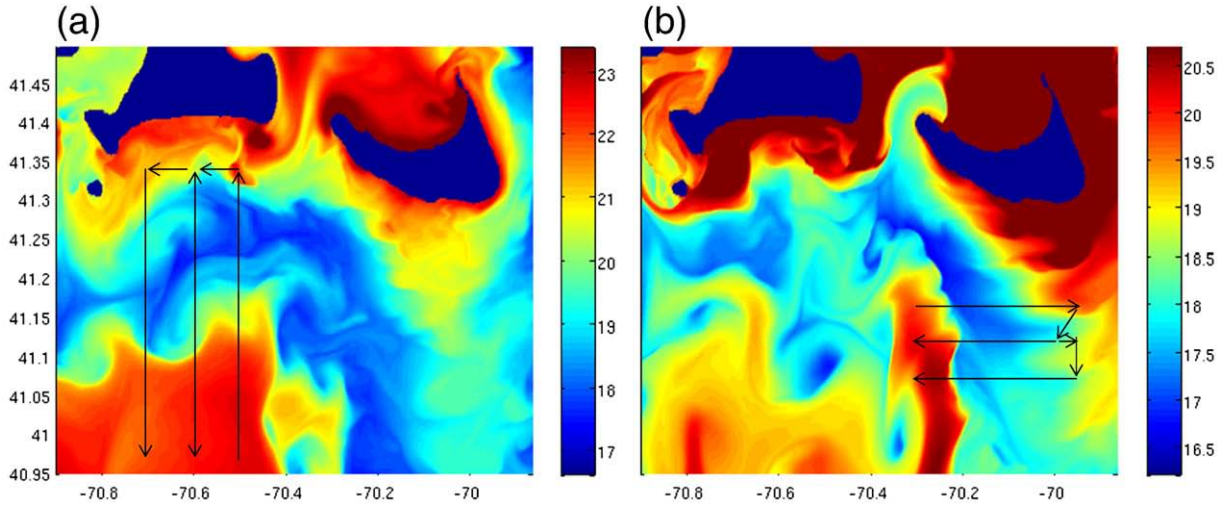

Fig. 9. NCOM-simulated SST on (a) 14 UTC 18 August 2003 and (b) 14 UTC 25 August. The black arrows denote selected tracks from the multiple flights of the Pelican aircraft as marked in Fig. 5. The observed and NCOM-simulated SSTs along these tracks are plotted in Fig. 18.

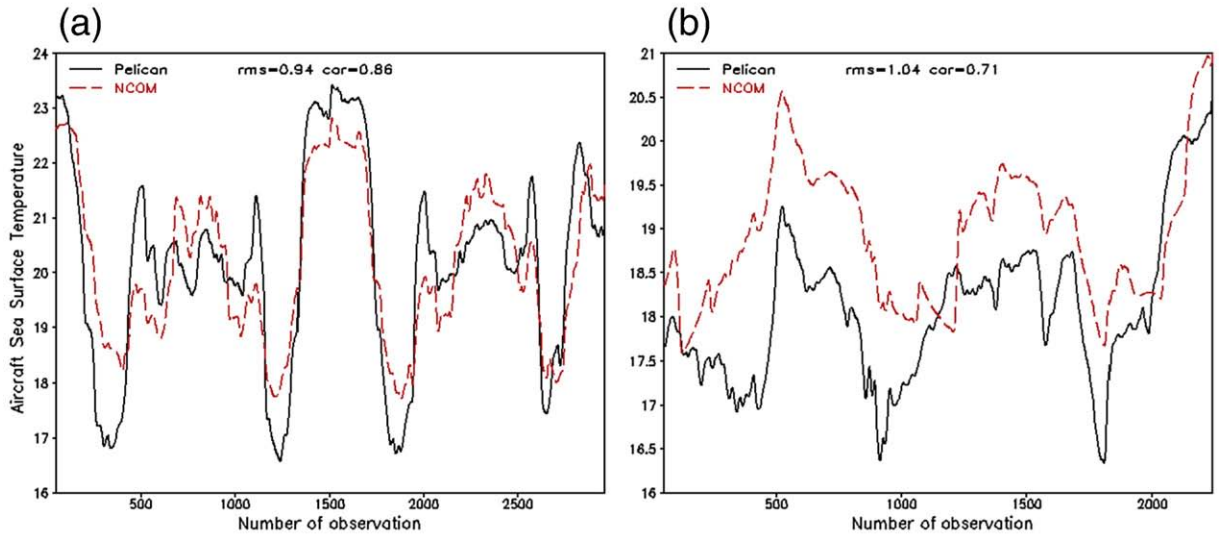

Fig. 10. Comparison of SST between observation by Pelican aircraft and NCOM simulation for (a) August 18 and (b) August 25, 2003.

surface waters are warm, with minimum cooling influence from the sustained tidal mixing during the sustained west/southwest wind period.

During the cooling event on August 18, a well-defined cold-water tongue is formed (Fig. 12c) partly due to the westward component of the wind accelerating the westward advection. The horizontal transport displayed in Fig. 13 denotes a westward transport south of the islands at this time. The transport is calculated during the model run and output at 24-hour intervals. The transport formulations are:

$$M_x = Du = \int_{-H}^{\xi} u\,dz$$
$$M_y = Dv = \int_{-H}^{\xi} v\,dz \quad (1)$$

where u and v are the current speeds in the east–west and north–south directions, H is the water depth, and ξ is the free-surface height. The cold-water transport to the south of Martha's Vineyard abruptly changes the local stratification.

A significant contribution to the cooling event is from heat lost during the passage of cool air through Muskeget Channel (Fig. 7b). Colder water in the northern part of the cold-water tongue near Muskeget Channel is within the footprint of the passage of cool air (Fig. 12c). Strong mixing induced by the heat loss can be found around 41.2°N along the cross section at 70.4°W (Fig. 12d). The negative heat flux erodes the surface stratification in the area of weaker stratification between the 25- and 40-m isobaths, enhancing the cold-water band and increasing the horizontal SST gradient south of Martha's Vineyard (Fig. 12c).

Table 2
Comparison of Pelican aircraft observed and NCOM modeled sea surface temperature (°C) for August 18 and 25, 2003.

	August 18, 2003		August 25, 2003	
	Pelican	NCOM	Pelican	NCOM
Mean	20.18	20.19	18.10	18.93
Standard deviation	1.82	1.43	0.85	0.83
Correlation	0.86		0.71	
RMS error	0.94		1.04	

Another process that may be involved in the cooling of the SST is upwelling. The vertical cross section along 41.13°N for August 18 is displayed in Fig. 14. The upwelling signature can be found in the column between 70.4 and 70.75°W. This upwelling corresponds to the gap-type wind directed to the southwest through Muskeget Channel. The warm surface waters are pushed southwestward following the wind direction. In the area of weak stratification, the colder waters in the deeper layers are upwelled to the surface.

The waters warm up and restratify again when the winds turn to the west/southwest after the cooling event on August 21 (Fig. 12e and Fig. 12f), and the horizontal gradient of the SST is significantly reduced south of Martha's Vineyard. The cold-water front has been pushed back further east. The SSTs are warmer in the perpetual cold-pool area due to the air–sea heat flux. Warm waters occupy most areas and the stratification south of Martha's Vineyard is restored to values similar to those that existed prior to the cooling event.

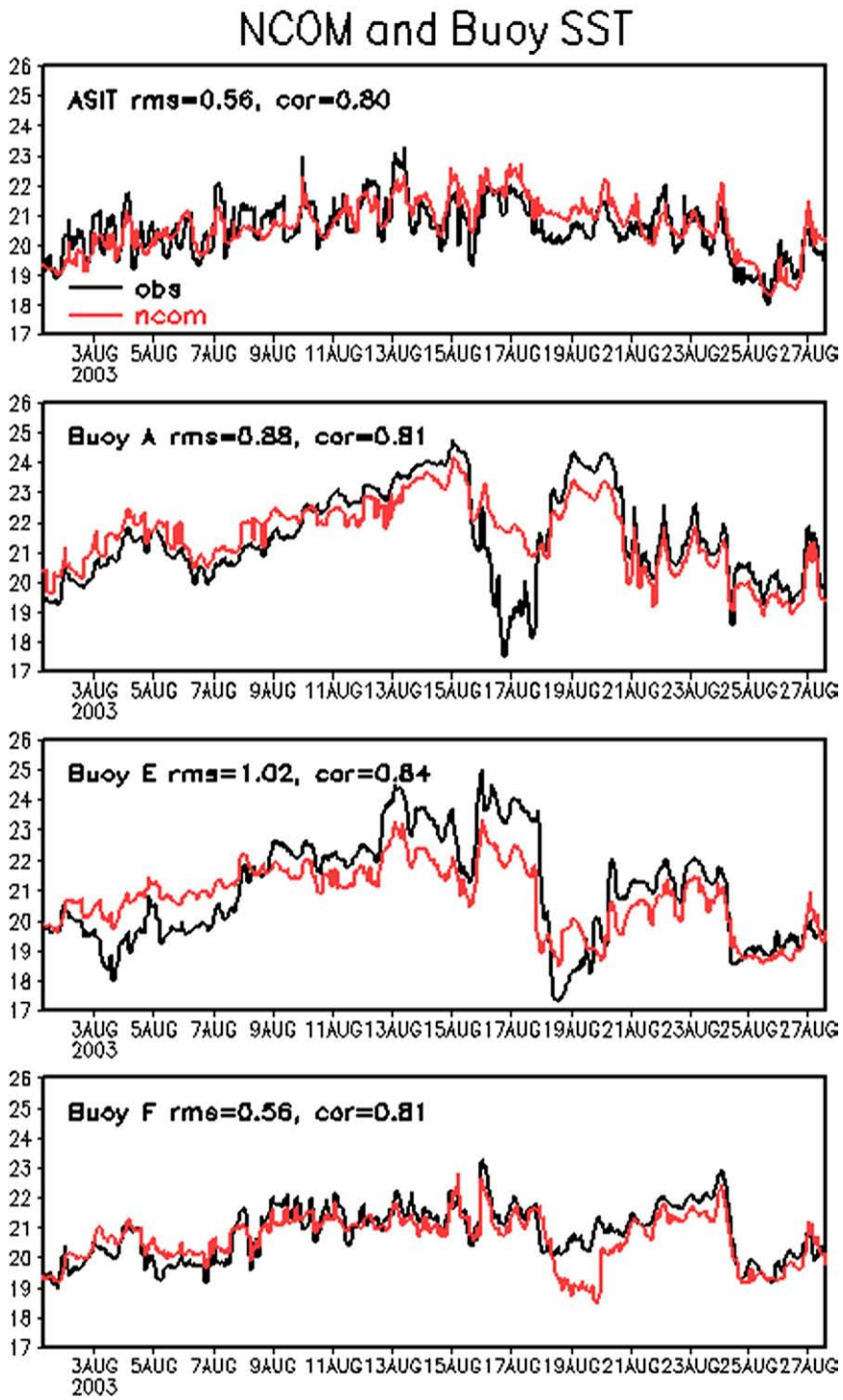

Fig. 11. Time series of observed and modeled SST at the locations of (a) ASIT, (b) mooring A, (c) mooring E, and (d) mooring F.

Table 3
Comparison of ASIT and IMET mooring observed and COAMPS modeled sea surface temperature (°C) for August 2003.

	ASIT	NCOM	Buoy A	NCOM	Buoy E	NCOM	Buoy F	NCOM
Mean	20.59	20.67	21.51	21.55	21.03	20.80	20.85	20.66
Standard deviation	0.87	0.90	1.51	1.19	1.72	1.17	0.90	0.82
Correlation	0.80		0.81		0.84		0.81	
RMS error	0.56		0.88		1.02		0.56	

7.2. Cooling event from August 24 to 25, 2003

The cooling event from August 24 to 25 has different wind directions from the August 17 to 18 cooling event. The winds in the study area are from the west before (August 23), northwest during (August 24), and southwest after (August 27) the cooling event (Fig. 8). The winds from the northwest have direction opposite that of the mean tidal flow. The unfavorable wind direction leaves the westward advection path of cold water less organized on August 25 (Fig. 15c) than on August 18 (Fig. 12c). The larger area of cooling is obviously due to the heat lost from the ocean to the atmosphere (Fig. 8b). The strong surface stratification (Fig. 15a and b) has been eroded by vertical mixing induced by strong surface cooling (Fig. 15c and d). The discontinuity along the westward transport channel indicates that the SST cooling (Fig. 15c) is related to the heat loss. Therefore, the winds have no major effect on the cooling of the local SST in their northwest direction since the horizontal transport induced by the local winds is eastward (Fig. 16), moving warmer water into the area and reducing the cooling of the surface layer. The cooling area is broader on August 25 than on August 18 corresponding to the extent of the air–sea heat flux. However, the vertical mixing on August 18 is stronger than that on August 25 due to the fact that the winds also contribute to the cooling.

After the cooling event, the west/southwest winds resume. The surface waters receive strong summer heat flux and warm up again (Fig. 15e) and the surface is recapped by warm water and the stratification is rebuilt (Fig. 15f).

The upwelling process seen on August 18 is not seen for the cooling event on August 25 (Fig. 17). The undisturbed temperature and density in the deeper layer does not indicate any surface forcing effect. The cooling in the surface layer is a result of the vertical

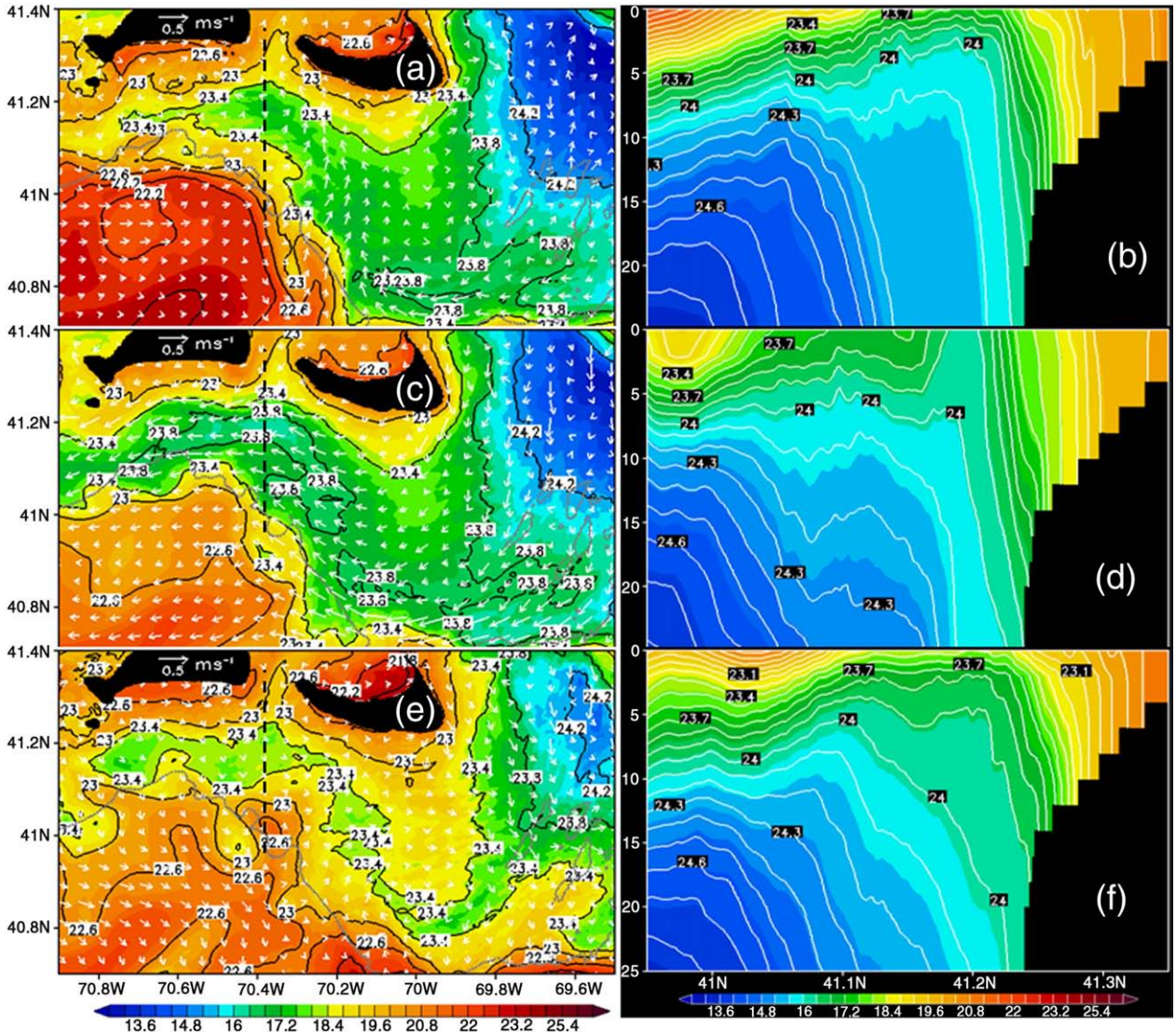

Fig. 12. NCOM daily mean surface temperature (°C, color contours), density (kg m^{-3}, black contour lines), and current (m s^{-1}, white vectors) on (a) August 16, (c) August 18, and (e) August 21. Vertical cross section of NCOM daily mean temperature (°C, color contours) and density (kg m^{-3}, white contour lines) on (b) August 16, (d) August 18, and (f) August 21 along 70.4°W. Dashed-lines in (a), (c), and (e) denote the corresponding positions for the cross sections in (b), (d), and (f). Gray dotted-lines in (a), (c), and (e) denote 40-m isobaths. (For interpretation of the references to color in this figure legend, the reader is referred to the web version of this article.)

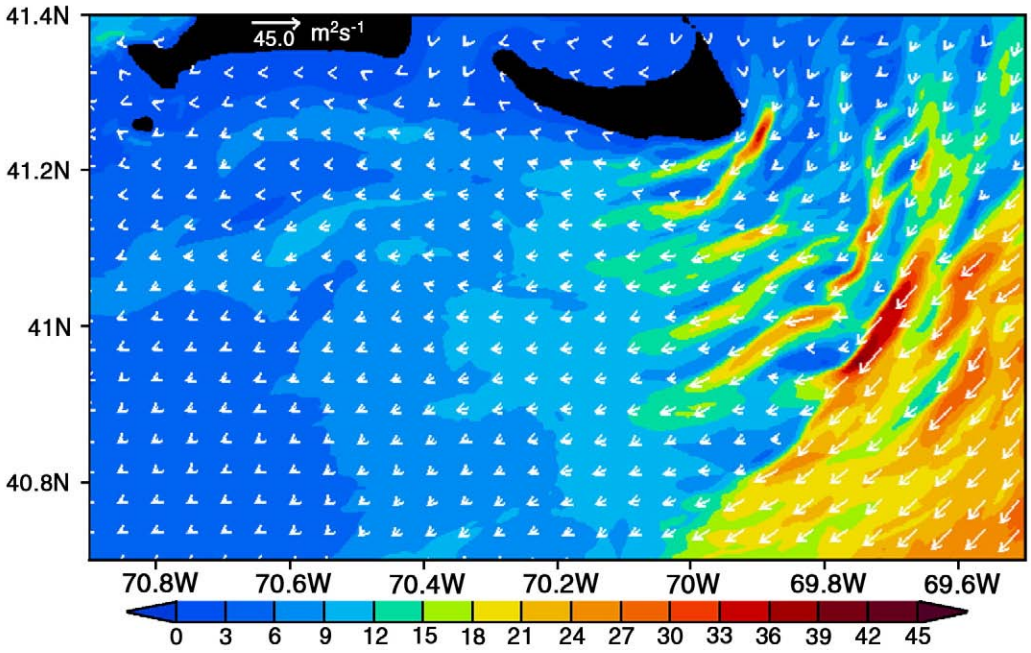

Fig. 13. Horizontal transport on August 18, 2003. The vectors display the size and direction of transport using east–west (M_x) and north–south (M_y) components in formulation (1). The magnitudes of the transport are plotted in color contours. (For interpretation of the references to color in this figure legend, the reader is referred to the web version of this article.)

mixing induced by the surface heat loss. The relatively uniformly-distributed vertical mixing near the surface along the center of the westward transport channel is the consequence of surface cooling in the larger area.

To compare the difference of the surface cooling from the cooling events between August 18 and 25, a scatter plot of density for the area having the most active response is shown in Fig. 18. The stronger response on August 18 is attributed to both the wind effect and the

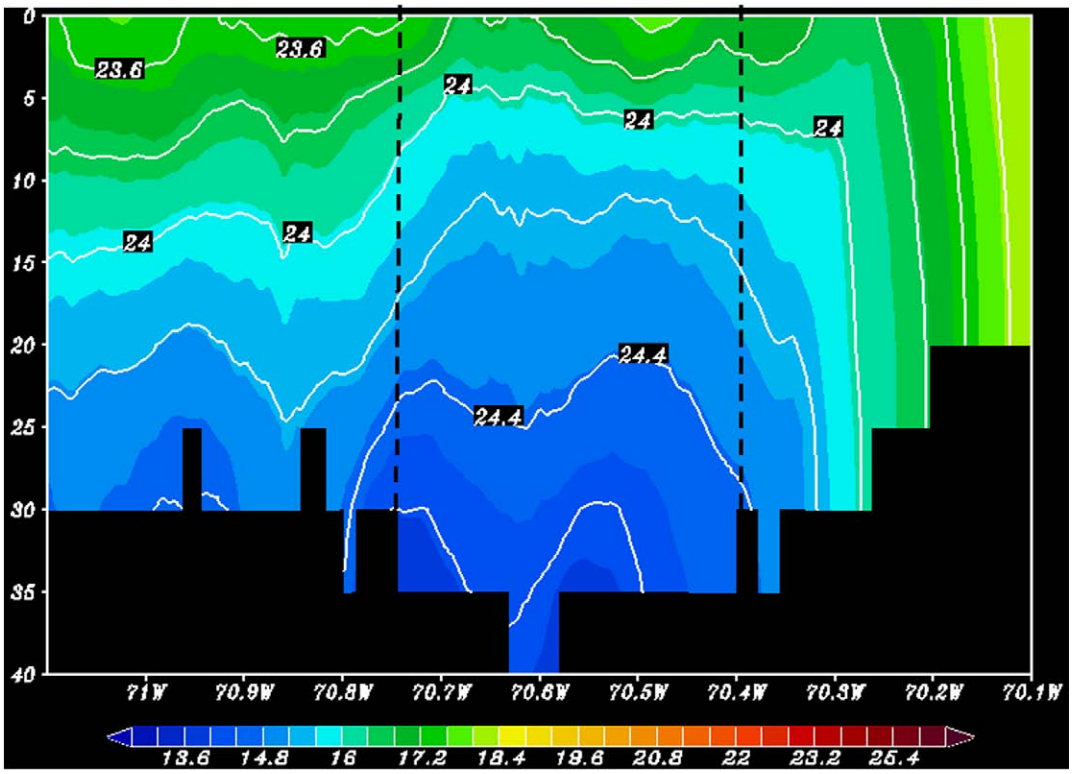

Fig. 14. Vertical cross section of NCOM daily mean surface temperature (°C, color contours) and density (kg m^{-3}, white contour lines) on August 18 along 41.13°N. Black dashed-lines indicate the areas used for the scatter plots in Fig. 18. (For interpretation of the references to color in this figure legend, the reader is referred to the web version of this article.)

surface heat loss. Although the surface heat loss is more significant and covers a larger area on August 25, the resulting water cooling is only confined to the surface layer. Since the northwest wind is not favorable for the westward transport of cold water, the wind has only a limited role in the cooling of the surface water on August 25.

8. Summary

Observations from AVHRR images, Pelican aircraft, the ASIT, and the IMET moorings are combined with a one-way-coupled numerical model simulation using COAMPS/NCOM to study the high SST variability that occurred during the summer of 2003 south of Martha's Vineyard. The mechanisms responsible for the high SST variability are investigated.

The COAMPS surface forcing fields, NCOM tides, and NCOM-simulated results are evaluated with the CBLAST-Low observations and the tidal-data-assimilative results of He and Wilkin (2006). At the ASIT, the mean and standard deviation of the winds and air–sea heat fluxes of COAMPS are comparable with the observations and the RMS errors with respect to the observations are reasonable. The correlations of the COAMPS air–sea heat fluxes and wind speed with the observed values exceed 0.87.

The comparisons of the tidal residual current speeds, amplitudes, and phases show that NCOM reasonably represents the eight tidal constituents used for the simulation. With highly-resolved bathymetry at high model resolution, some significant tidal features, such as cyclonic eddies related to the sand troughs on Nantucket Shoals, are presented in the tidal analyses.

The NCOM-simulated SSTs generally match the observations along the Pelican aircraft track. The RMS errors on August 25 are slightly larger than those on August 18, in correspondence with the less organized features of the cold-water westward transport on August 25. At the ASIT and at the IMET moorings, the NCOM SSTs match the SST observations fairly well for the month of August, except at the sites where the observed SST undergoes vigorous changes during the cooling event in the warm summer season and the NCOM simulation has larger RMS errors.

The Pelican aircraft data show that the horizontal gradient of SST can be as large as 6 °C over 5 km, with a tongue of water colder than 17 °C penetrating ambient water of 23 °C on August 18, 2003 south of Martha's Vineyard. Corresponding to the high SST variability, the data from both the ASIT observations and the COAMPS predictions show that the atmospheric surface fluxes and wind speeds are peculiar to the summer warm season in this area. Two cooling events, from August 17 to 18 and from August 24 to 25, are found to be related to the high SST variability. The heat lost from the ocean through the surface is more significant from August 24 to 25 than from August 17 to 18, with a maximum difference of about 200 W m^{-2} based on the ASIT observations. The local northerly winds during these two time periods, however, vary from northeast associated with a high-

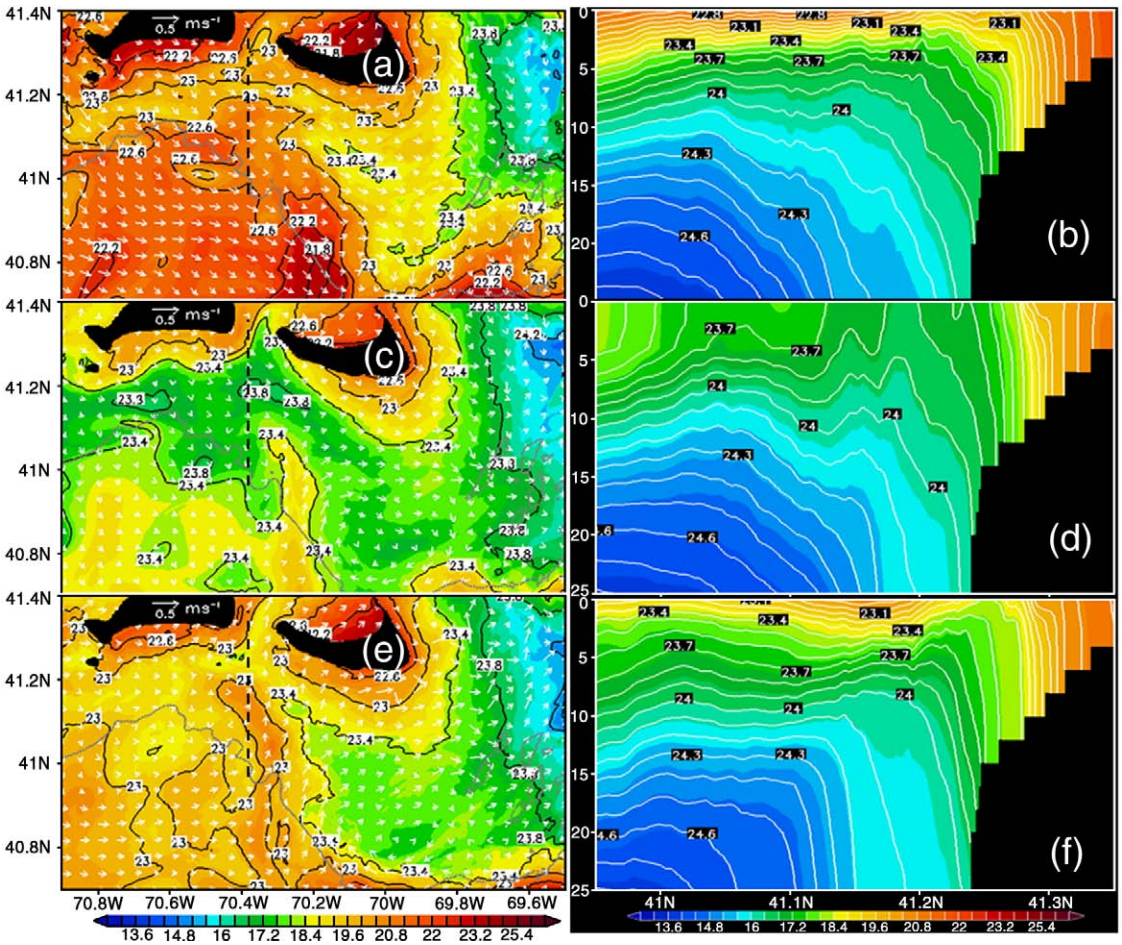

Fig. 15. NCOM daily mean SST (°C, color contours), density (kg m^{-3}, black contour lines) and current (m s^{-1}, white vectors) on (a) August 23, (c) August 25, and (e) August 27. Vertical cross section of NCOM daily mean temperature (°C, color contours) and density (kg m^{-3}, white contour lines) on (b) August 23, (d) August 25, and (f) August 27 along 70.4°W. Dashed-lines in (a), (c) and (e) denote the corresponding positions for the cross sections in (b), (d), and (f). Gray dotted-lines in (a), (c), and (e) show 40-m isobaths. (For interpretation of the references to color in this figure legend, the reader is referred to the web version of this article.)

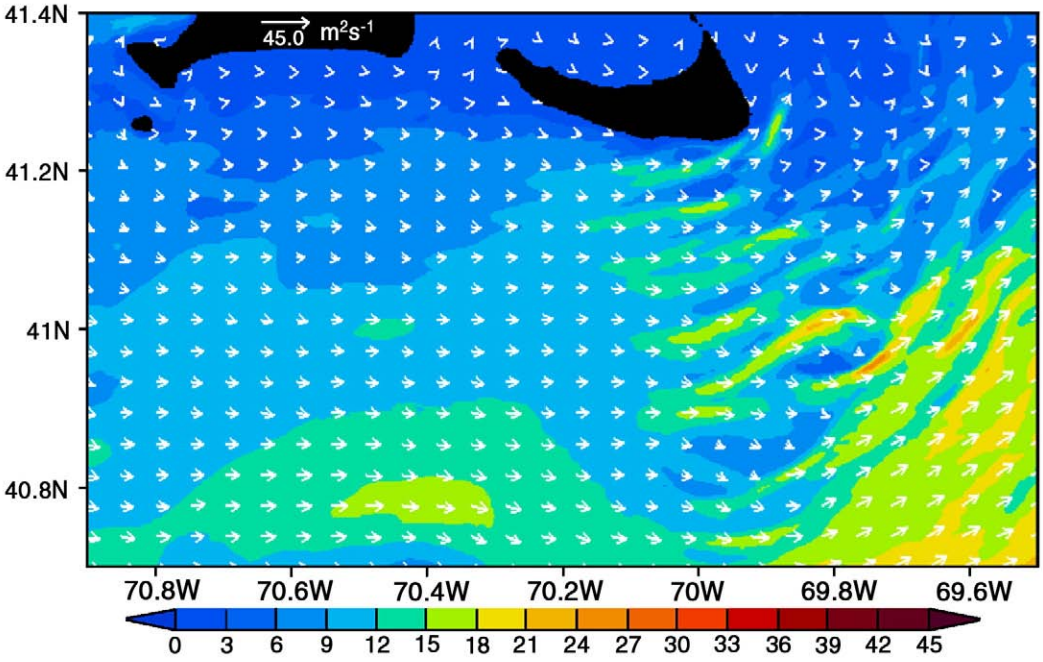

Fig. 16. Same as Fig. 13 except for horizontal transport on August 25, 2003.

pressure system passage on August 18 to northwest associated with a low-pressure system passage on August 24.

The NCOM results display sustained strong stratification south of Martha's Vineyard during August, except during cooling events from August 17 to 18 and from August 24 to 25. High SST variability occurs on August 18 and 25 due to the cold water that appeared in the warm and stratified water.

The NCOM simulation suggests that the high SST variability observed on August 18 is strongly related to the surface winds and air–sea heat fluxes. The northeast winds expedite the westward

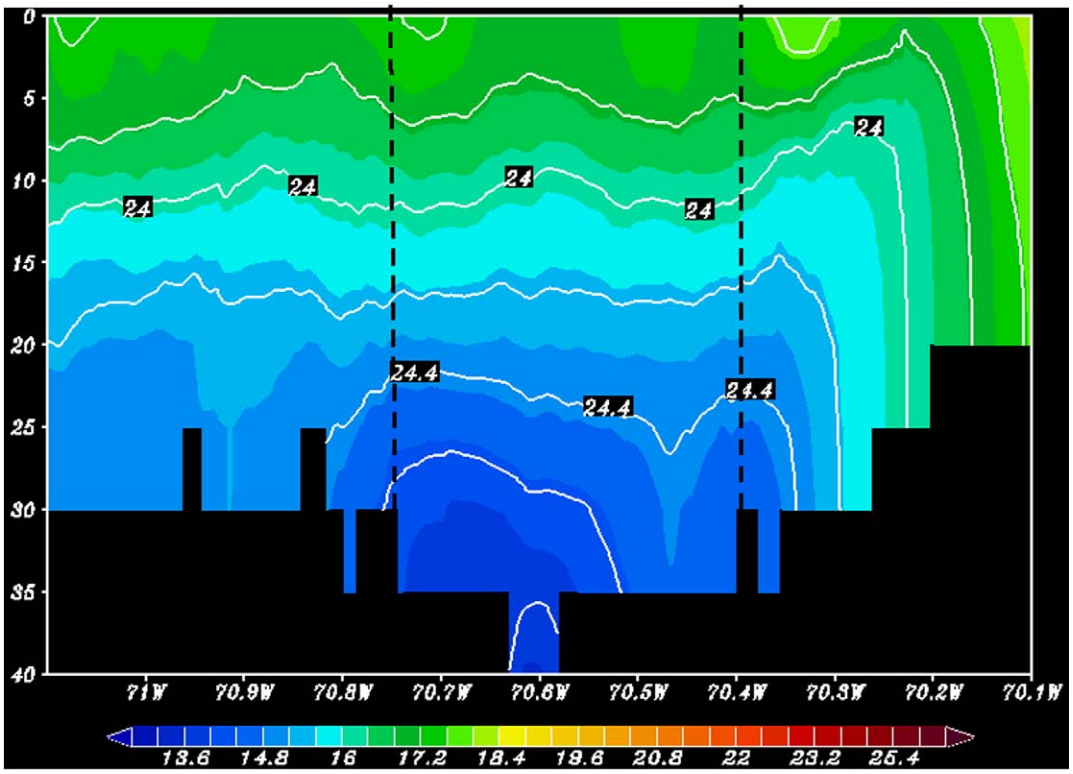

Fig. 17. Vertical cross section of NCOM daily mean surface temperature (°C, color contours) and density (kg m^{-3}, white contour lines) on August 25 along 41.13°N. Black dashed-lines indicate the areas for the scatter plots in Fig. 18. (For interpretation of the references to color in this figure legend, the reader is referred to the web version of this article.)

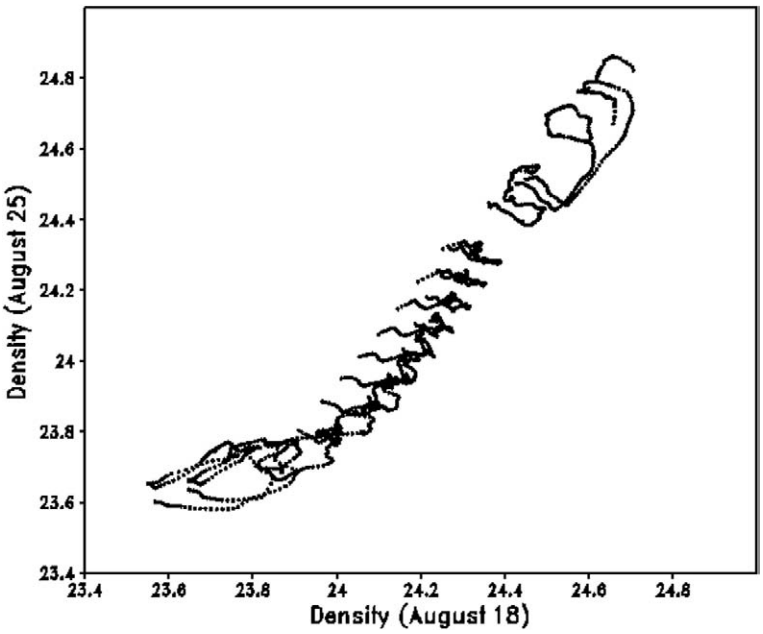

Fig. 18. Scatter plots for NCOM daily mean density in the area marked in Fig. 14 and 17. The *x*-axis denotes the mean density for August 18 and the *y*-axis for August 25.

advection of cold water originating from the cold water on the east flank of Nantucket Shoals and form a narrow tongue of cool water. The cooling event further induces vertical mixing by the heat loss and upwelling by the northeast gap-type wind through Muskeget Channel and enhances the local decrease of the SST along the cool tongue.

The SST variability on August 24 to 25 is due to somewhat different processes. The local winds, which are northwest, show no major effect on the cooling of the local SST, since the horizontal transport induced by these winds is eastward, moving warmer water into the area south of Martha's Vineyard and reducing the cooling of the surface layer. The cooling occurs over a broad area corresponding to extent of the air–sea heat fluxes and is more related to vertical mixing induced by surface cooling. Even though stronger winds and greater heat loss occur, the surface waters are less dense, indicating weaker response to the surface cooling on August 25 than on August 18.

This study reveals the complex processes causing the high SST variability south of Martha's Vineyard. The processes include tidal currents, tidal and wind-driven advection, air–sea fluxes, vertical mixing, and upwelling. Strong tidal currents generate a perpetual cool pool on the east flank of Nantucket Shoals by vertical mixing. This cold water is advected westward by the tidal residual flow. Surface winds can either accelerate (on August 18) or decelerate (on August 25) this transport, depending on the wind direction and can also generate upwelling (on August 18) when the local stratification is weak. In addition, vertical mixing induced cooling can be caused by the ocean surface heat loss to the atmosphere as occurred on August 18.

Although the model results have been verified quantitatively with the observations, the studies of possible processes controlling the sharp and small-scale SST variations are based on qualitative comparisons between the spatial structures of the variables. Further investigation is needed to quantitatively identify the contributions and relative importance of the different processes.

Since the formation of high SST variability south of Martha's Vineyard involves strong air–ocean interaction, the investigation of this area could benefit from the use of a two-way-coupled ocean–atmosphere model to provide feedback of the ocean-model-predicted SST to the atmospheric-model-computed air–sea heat fluxes and wind stresses.

Acknowledgments

The support of the sponsors, the Office of Naval Research, Ocean Modeling and Prediction Program, through program element 8068085 is gratefully acknowledged. We thank Pelican Research Aircraft team for SST measurement. Computations were performed on the IBM P4+ at the Naval Oceanographic Office (NAVO) Major Shared Resource Center (MSRC) at Stennis Space Center, Mississippi.

References

Barron, C.N., Kara, A.B., Martin, P.J., Rhodes, R.C., Smedstad, L.F., 2006. Formulation, implementation and examination of vertical coordinate choices in the global Navy Coastal Ocean Model (NCOM). Ocean Modelling 11, 347–375. doi:10.1016/j.ocemod.2005.01.004.

Bishop, C.H., Toth, Z., 1999. Ensemble transformation and adaptive observations. Journal of the Atmospheric Sciences 56, 1748–1765.

Bishop, C.H., Etherton, B.J., Majumdar, S.J., 2001. Adaptive sampling with the ensemble Kalman Filter, I: theoretical aspects. Monthly Weather Review 129, 420–436.

CBLAST low log 2003. http://www.whoi.edu/science/AOPE/CBLAST/CBLAST%20LOW%20LOG.htm.

Chao, Y., Zhijin, L., Kindle, J.C., Paduan, J.D., Chavez, F.P., 2003. A high-resolution surface vector wind product for coastal oceans: blending satellite scatterometer measurements with regional mesoscale atmospheric model simulations. Geophysical Research Letters 30 (No. 1), 1013. doi:10.1029/2002GL015729.

Cummings, J.A., 2005. Operational multivariate ocean data assimilation. Quarterly Journal of the Royal Meteorological Society 131, 3583–3604.

Divins, D.L., Metzger, D., 2008. NGDC coastal relief model. National Geophysical Data Center. WWW page, http://www.ngdc.noaa.gov/mgg/coastal/coastal.html.

Donlon, C., et al., 2007. The global ocean data assimilation experiment high-resolution sea surface temperature pilot project. Bulletin of the American Meteorological Society 88 (8), 1197–1213.

Edson, J.B., et al., 2007. The coupled boundary layers and air–sea transfer experiment in low winds (CBLAST-LOW). Bulletin of the American Meteorological Society 88 (3), 341–356.

Egbert, G.D., Bennett, A.F., Foreman, M.G.G., 1994. TOPEX/Poseidon tides estimated using a global inverse model. Journal of Geophysical Research 99, 24821–24852.

Farrar, J.T., Zappa, C.J., Weller, R.A., Jessup, A.T., 2007. Sea surface temperature signatures of oceanic internal waves in low winds. Journal of Geophysical Research 112, C06014. doi:10.1029/2006JC003947.

He, R., Wilkin, J.L., 2006. Barotropic tides on the southeast New England shelf: a view from a hybrid data assimilative modeling approach. Journal of Geophysical Research 111, C08002. doi:10.1029/2005JC003254.

Hodur, R.M., Hong, X., Doyle, J.D., Pullen, J.D., Cummings, J.A., Martin, P.J., Rennick, M.A., 2002. The coupled ocean/atmosphere mesoscale prediction system (COAMPS). Oceanography 15 (No. 1), 88–89.

Hong, X., Cummings, J.A., Martin, P.J., Doyle, J.D., 2009. Ocean data assimilation: a coastal application. In: Parks, S., Xu, L. (Eds.), Data Assimilation for Atmospheric, Oceanic and Hydrologic Applications. Springer, pp. 267–290.

Hong, X., Bishop, C.H., 2005. COAMPS Ocean Ensemble Forecast System. WWW page, http://ams.confex.com/ams/WAFNWP34BC/techprogram/paper_94771.htm.
Hong, X., Bishop, C.H., 2006. COAMPS Ocean Ensemble Forecast and Adaptive Sampling System. WWW page, http://www.agu.org/meetings/os06/cd/.
Hong, X., Hodur, R.M., Martin, P., 2007. Numerical simulation of deep-water convection in the Gulf of Lion. Pure and Applied Geophysics 164, 2101–2116.
Jerlov, N.G., 1976. Marine Optics. Elsevier. 231 pp.
Khelif, D., Jonsson, H., Friehe, C., 2004. Marine Atmospheric Boundary-Layer Structure and Air–Sea Fluxes During CBLAST-Low. WWW page, http://wave.eng.uci.edu/files/cblast/docs/36x72_khelif_ams_blt_2004.pdf.
Kondo, J., 1975. Air–sea bulk transfer coefficients in diabatic conditions. Boundary-Layer Meteorology 9, 91–112.
Martin, P.J., 2000. Description of the navy coastal ocean model version 1.0. Naval Research Laboratory 1–42 NRL/FR/7322-00-9962.
Martin, P.J., Hodur, R.M., 2003. Mean COAMPS Air–Sea Fluxes Over the Mediterranean During 1999 Report. Naval Research Laboratory, Stennis Space Center, Mississippi.
Martin, P.J., Book, J.W., Doyle, J.D., 2006. Simulation of the northern Adriatic circulation during winter 2003. Journal of Geophysical Research 111, C03S12. doi:10.1029/2006JC003511.
Morey, S.L., Martin, P.J., O'Brien, J.J., Wallcraft, A.A., Zavala-Hidalgo, J., 2003. Export pathways for river discharge fresh water in the northern Gulf of Mexico. Journal of Geophysical Research 108, 3303. doi:10.1029/2002JC001674.
Nachamkin, J.E., 2004. Mesoscale verification using meteorological composites. Monthly Weather Review 132, 941–955.
Pullen, J.D., Doyle, J.D., Hodur, R.M., Ogston, A., Book, J.W., Perkins, H., Signell, R., 2003. Coupled ocean–atmosphere nested modeling of the Adriatic Sea during winter and spring 2001. Journal of Geophysical Research 108 (C10), 3320. doi:10.1029/2003JC001780.
Shulman, I., Kindle, J., Martin, P.M., deRada, S., Doyle, J.D., Penta, B., Anderson, S., Chavez, F., Paduan, J., Ramp, S., 2007. Modeling of upwelling/relaxation events with the Navy Coastal Ocean Model. Journal of Geophysical Research 112, C06023. doi:10.1029/2006JC003946.
Thompson, D.R., Monaldo, F.M., Farrar, J.T., Weller, R.A., Elfouhaily, T.M., Grimmett, T.M., 2004. Comparison of high-resolution wind maps from SAR imagery with *in situ* measurements from the ONR CBLAST experiments. IEEE International Geoscience and Remote Sensing Symposium 40–43 Anchorage, AK, (Sep 2004).
Vickers, D., Mahrt, L., 2006. Evaluation of the air–sea bulk formula and sea-surface temperature variability from observations. Journal of Geophysical Research 111 (C05002). doi:10.1029/2005JC003323.
Wang, S., Wang, Q., Gao, Z., Edson, J.B., Weller, R., Helmis, C. 2004. Evaluation of COAMPS real time forecast for CBLAST-Low summer experiments 2002/2003. Preprints, 16th Symposium On Boundary Layers and Turbulence, Portland, ME, Amer. Meteor. Soc., CD-ROM, P8.2.
Wilkin, J., 2006. The summertime heat budget and circulation of southeast New England Shelf waters. Journal of Geophysical Research 36, 1997–2011.